

Graphical X Splatting (GraphiXS): A Graphical Model for 4D Gaussian Splatting under Uncertainty

DOĞA YILMAZ, University College London, United Kingdom

JIALIN ZHU, Baidu Research, China

DESHAN GONG, The University of Hong Kong, China

HE WANG*, University College London, United Kingdom

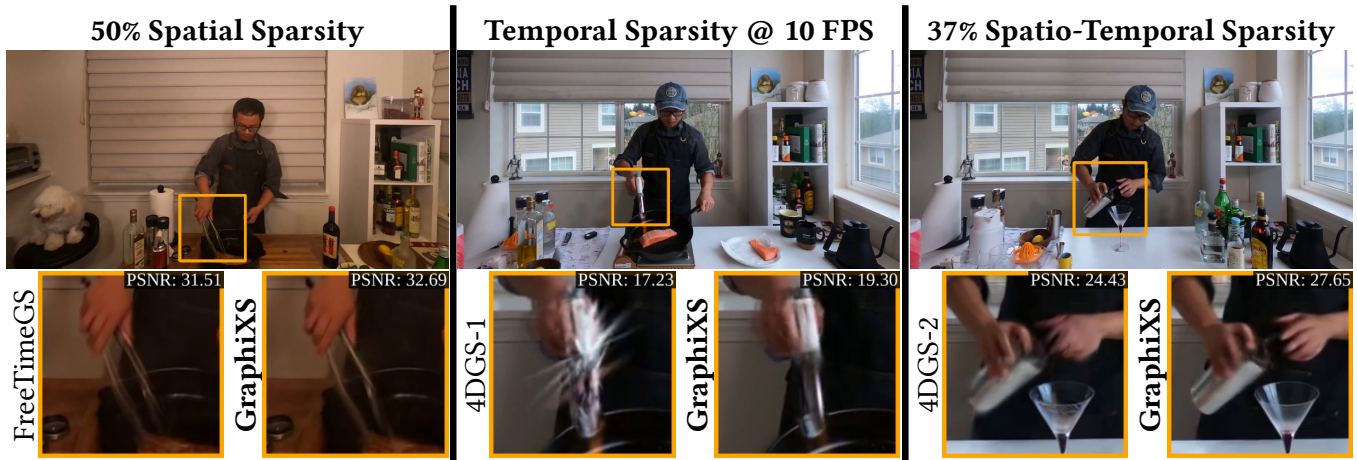


Fig. 1. GraphiXS outperforms existing 4DGS methods under various types of data uncertainty. Left: 50% cameras missing; Middle: 10 FPS low-speed cameras; Right: 37% random frames missing.

We propose a new framework to systematically incorporate data uncertainty in Gaussian Splatting. Being the new paradigm of neural rendering, Gaussian Splatting has been investigated in many applications, with the main effort in extending its representation, improving its optimization process, and accelerating its speed. However, one orthogonal, much needed, but under-explored area is data uncertainty. In standard 4D Gaussian Splatting, data uncertainty can manifest as view sparsity, missing frames, camera asynchronization, *etc.* So far, there has been little research to holistically incorporating various types of data uncertainty under a single framework. To this end, we propose Graphical X Splatting, or *GraphiXS*, a new probabilistic framework that considers multiple types of data uncertainty, aiming for a fundamental augmentation of the current 4D Gaussian Splatting paradigm into a probabilistic setting. *GraphiXS* is general and can be instantiated with a range of primitives, *e.g.* Gaussians, Student's-t. Furthermore, *GraphiXS* can be used to 'upgrade' existing methods to accommodate data uncertainty. Through exhaustive evaluation and comparison, we demonstrate that *GraphiXS* can systematically model various uncertainties in data, outperform existing methods in many settings where data are missing or polluted in space and time, and therefore is a major generalization of the current 4D Gaussian Splatting research.

CCS Concepts: • Computing methodologies → Machine learning approaches; Rendering.

*Corresponding author.

Authors' Contact Information: Doğa Yılmaz, University College London, London, United Kingdom, doga.yilmaz@ucl.ac.uk; Jialin Zhu, Baidu Research, Beijing, China, misaliet@outlook.com; Deshan Gong, The University of Hong Kong, Hong Kong, China, deshan@hku.hk; He Wang, University College London, London, United Kingdom, he_wang@ucl.ac.uk.

Additional Key Words and Phrases: Gaussian Splatting, Graphical Models, Bayesian Inference

1 Introduction

As the latest paradigm of 3D reconstruction and neural rendering, Gaussian Splatting (GS) has served as a fundamental component of many systems [Xiang et al. 2025; Zhou et al. 2024]. At the high level, the current research effort can be broadly categorized as extending the representation [Hamdi et al. 2024; Liu et al. 2025b; Zhu et al. 2025], designing new optimization strategies [Kheradmand et al. 2024; Kim et al. 2025; Zhu et al. 2025], speeding inference processes or/and scaling up the model [Feng et al. 2025; Kerbl et al. 2024; Mallick et al. 2024]. The three lines of research have spawned new applications in novel view synthesis [Xie et al. 2024; Yang et al. 2025], SLAM [Matsuki et al. 2024], geometric reconstruction [Dai et al. 2024; Huang et al. 2024], *etc.*

One under-explored theme that is orthogonal to all the aforementioned research is data uncertainty, which universally exists in real-world applications. Taking multi-view 4DGS as an example, most existing research focuses on learning the dynamics of Gaussian components, with the aim of high reconstruction quality [Wu et al. 2024; Yang et al. 2024b], generalization on unseen motions [Li et al. 2024; Zhu et al. 2024], large complex 3D scenes [Xie et al. 2025], *etc.* However, all of them explicitly or implicitly assume that sufficient data can be obtained with high quality. In practice, this often means enough cameras with views covering all angles, and good camera

calibration and synchronization. We argue that such assumptions can be too restrictive as the data collection setup can be constrained by many factors such as security, safety, operational constraints, *e.g.* cameras at traffic junctions might only cover a few angles.

Recently, some methods, including contemporaneous ones, have started to consider certain data uncertainties in GS. This includes probabilistic inference for online learning [Guo et al. 2025; Savant et al. 2024; Van de Maele et al. 2024], dynamically learning moving and static Gaussians [Deng et al. 2025; Gao et al. 2024; Wang et al. 2025a], reconstruction from limited camera views [Jeong et al. 2024; Jiang et al. 2023; Yilmaz and Kiraç 2023]. However, the data uncertainty explicitly or implicitly considered is mostly specific to one application scenario. Therefore, it is desirable to have one unified framework that can incorporate multiple types of data uncertainty.

We propose Graphical X Splatting (GraphiXS), a new framework which can explicitly incorporate multiple types of data uncertainty in 4DGS. The ‘X’ in GraphiXS is not necessarily Gaussian so we use the word ‘component’. The term ‘data uncertainty’ broadly refers to missing camera views, sparse camera configurations (*i.e.* position and orientations), missing frames from cameras, imperfectly synchronized cameras, *etc.* Probabilistic learning is a natural solution to data uncertainty, but the greatest challenge is to design a flexible probabilistic framework that can model different types of uncertainty in 4DGS. To this end, we formulate GraphiXS as a generative process and propose a new graphical model, by introducing stochasticity into the individual steps of 4DGS. This includes treating all the learnable parameters (*e.g.* component location) as latent variables which are to be inferred via Maximum a Posteriori (MAP). Also, unlike existing methods which treat only the images as observations, we also treat the camera pose and frame time as samples of random variables, which enables us to incorporate the uncertainty in them. Finally, the flexibility of GraphiXS allows us to impose various prior distributions to regulate the behaviors of the components.

We instantiate GraphiXS with different components including Gaussians and Student’s-t to show its generality. Through exhaustive evaluation under various combinations of data uncertainty, we demonstrate that GraphiXS can outperform existing methods across different scenes and metrics. More broadly, we demonstrate that GraphiXS is not a specific model but a framework which can be used to upgrade and improve existing methods. To the best of our knowledge, this is the first probabilistic 4DGS framework targeting multiple types of data uncertainty. Our contributions include:

- A new probabilistic framework to holistically incorporate data uncertainty in 4DGS.
- A new graphical model which can be instantiated with different primitives and used to ‘upgrade’ existing 4DGS methods.
- A new way of introducing stochasticity in the steps of 4DGS.
- New priors that can effectively regulate the model behaviors, leading to effective optimization.

2 Related Work

Traditional Methods. Multi-View Stereo (MVS) [Seitz et al. 2006] is well studied before deep learning. Software such as Colmap [Schönenberger et al. 2016] has been widely utilized in 3D reconstruction. It reconstructs the geometrically consistent points between images and

restores camera poses by calculating corresponding features in images from multiple perspectives. Denser and more precise geometries can be obtained using the Structure from Motion (SFM) [Ullman 1979]. Meanwhile, additional data (*e.g.* depth) captured from Time of Flight (ToF) or Light Detection And Ranging (Lidar) sensors can be accessed from some other methods such as SLAM [Bailey and Durrant-Whyte 2006; Durrant-Whyte and Bailey 2006] and Kinect-Fusion [Newcombe et al. 2011] for 3D reconstruction.

Learning-based Reconstruction Method. For a single scene, there are two main cornerstone methods in this sub-area: Neural Radiance Field (NeRF) [Mildenhall et al. 2021] and 3D Gaussian Splatting (3DGS) [Kerbl et al. 2023]. NeRF utilizes a neural network to implicitly learn the 3D radiance field. It can achieve novel view synthesis by querying different points’ color and density values from the neural network. NeRF accomplishes good reconstruction results, but its rendering efficiency is low, making it unsuitable for real-time rendering tasks. Comparatively, 3DGS can achieve real-time rendering, but requires more memory compared with NeRF. 3DGS uses 3D Gaussians as components in space. To optimize their attributes (means, covariances, colors, *etc.*), it uses a rasterization method called Splatting [Zwicker et al. 2002] to obtain rendering results from different perspectives. Many subsequent methods are then proposed to improve 3DGS. Among them, some attempt to improve 3DGS in the fundamental paradigm, *e.g.* using different primitives other than Gaussian including SSS [Zhu et al. 2025], DBS [Liu et al. 2025b], and 2DGS [Huang et al. 2024], while others try to improve the training processing and adaptive density control in vanilla 3DGS, such as sampling-based [Kheradmand et al. 2024; Kim et al. 2025; Zhu et al. 2025] methods, elevating rendering quality to a new level.

Dynamic Reconstruction. Most traditional methods either perform a frame-by-frame reconstruction and lack motion continuity, or require calculating optical flow maps to simulate dynamics but cannot reconstruct dense scene flows. In comparison, dynamic reconstruction based on NeRF and 3DGS yields better results. D-NeRF [Pumarola et al. 2021] extend NeRFs to dynamic scenes by introducing an MLP to learn the implicit deformation field in every time interval for the motion. Because of the good learning capability of the implicit representation of NeRF, most NeRF-based dynamic reconstruction methods adopt concepts that are similar to D-NeRF. On the other hand, there are currently two main threads for dynamic reconstruction using 3DGS-based methods. The first is learning the trajectories of explicit primitives at different times. Deformable 3DGS [Yang et al. 2024a] and 4DGS-2 [Wu et al. 2024] follow the idea of D-NeRF, using neural networks/Tri-planes/HexPlanes to learn the motion and deformation of 3D Gaussians. MotionGS [Zhu et al. 2024], SplineGS [Park et al. 2025], and FreetimeGS [Wang et al. 2025b], on the other hand, simulate the dynamics of 3D Gaussians in space through optical flow, spline, and linear flow. The second thread involves building higher-dimensional primitives based on the properties of explicit primitives in the 3DGS method. Then, these properties of primitives at different times in 3D space can be calculated by marginalizing the time dimension. Research such as 4DGS-1 [Yang et al. 2024b], 7DGS [Gao et al. 2025], and UBS [Liu et al. 2025a] are all under this direction.

Uncertainty in Reconstruction. Existing works such as SGS [Savant et al. 2024] and USPLAT4D [Guo et al. 2025] have attempted to improve reconstruction quality by estimating the uncertainty of primitives in Gaussian Splatting. However, only few methods take into account the inherent uncertainty of the training data besides the primitive uncertainty. Yang et al. [2024a] argued that inaccuracies in pose estimation can cause spatial jitter between frames. Research including LongSplat [Lin et al. 2025], DG-SLAM [Xu et al. 2024] and GS-CPR [Liu et al. 2024] adjusts camera poses during the training process. Besides, Bui et al. [2025] pointed out that the temporal uncertainty should not be neglected, especially for the photon integration process within the physical shutter time. Nevertheless, there is no work modeling further data uncertainty such as asynchronous cameras and performing probabilistic modeling of multiple types of uncertainty for 4DGS.

3 Methodology

3.1 Preliminaries

3.1.1 3D/4DGS as a mixture model. GS utilizes a large number of 3D Gaussian components to fit a 3D radiance field. Each component is represented by

$$G(x) = e^{-\frac{1}{2}(x-\mu)^T \Sigma^{-1}(x-\mu)} \quad (1)$$

where μ and Σ are the location and shape (with truncation). In addition, each component has additional attributes, including opacity o , and color s which is based on spherical harmonics sh . During rendering, each 3D Gaussian is transformed into a 2D Gaussian on the image plane. The rendering is then computed by:

$$C(d) = \sum_{i=1}^N s_i o_i G_i^{2D}(d) \prod_{j=1}^{i-1} (1 - o_j G_j^{2D}(d)). \quad (2)$$

where $C(d)$ is the final color of the d th pixel, N is the number of the Gaussians that intersect with the ray cast from the pixel. All Gaussian parameters are learned from the 2D images.

Essentially 3D/4DGS can be seen as learning a (unnormalized) mixture model with Gaussians [Zhu et al. 2025]:

$$F(x) = \sum w_i G_i(x) \quad (3)$$

where w_i is determined by o_i , s_i and the rendering process. Our GraphiXS generalizes this concept by a new graphical model and a corresponding generative process based on the mixture model.

3.1.2 Graphical model. Graphical Model is a probabilistic model which uses a graph to express the conditional dependencies of random variables. It allows structured dependencies to be introduced among random variables to describe a data generation process. Then the knowledge of this process can be used as inductive bias for model design. This is particularly suitable for 4DGS since it describes a multi-step process of rendering (Eq.1-3) and each step involves several quantities which can be treated as random variables. Also, Graphical Model naturally enables Bayesian inference. This is achieved by factorizing the joint probability of all variables into a series of conditional probabilities based on the graph, each of which can be independently modeled and evaluated. For a complex process like 4DGS, as shown later, this provides the flexibility for us to design separate priors to regulate overall model behaviors. Below, we first

introduce the graphical model and its corresponding generative process, followed by model decomposition. Then we explain how to model each of the terms in the model. Lastly, we derive the final loss function for training.

3.2 GraphiXS as a Graphical Model

Notations. Given videos in a multi-view setting, we aim to reconstruct the 4D radiance field. We define random variables C for the cameras pose, T for frame time, I for video frame with pixels X . The data consists of M camera poses, each recording K frames, giving a total of $M \times K$ frames and each frame with D pixels. We use superscripts for time, superscripts with brackets for derivatives, and subscripts for other indices, e.g. $X_{c,d}^t$ indicates the d th pixel of the image I_c^t from camera c at time t .

Our new GraphiXS is a graphical model (Fig. 2) which represents a generative process from a (unnormalized) mixture model with a potentially infinite number of components $F = \sum_{i=1}^N \delta_{\theta_i}$, where $N \rightarrow +\infty$ and δ_{θ_i} is the i th component parameterized by θ_i . The generative process is then described as follows:

- (1) Given the mixture model F , a camera $c \sim C$ and a time $t \sim T$, sample a subset of F which is called $\{\alpha_i\}$ with L components, for an image I_c^t .
- (2) For every $X_{c,d}^t \in I_c^t$ indexed by c , t , and d , sample a ray $R_{c,d}^t$.
- (3) Given $\{\alpha_i\}$ and $R_{c,d}^t$, sample a subset of $\{\alpha_i\}$ which is called $\{\beta_j\}$ with A components.
- (4) Finally, generate the color for $X_{c,t}^t$ based on $\{\beta_j\}$ and $R_{c,d}^t$.

Figure 2 describes most of the existing GS work where some steps are realized as rule-based deterministic processes. For instance, the original 3DGS is special case of GraphiXS without T and with δ_{θ_i} being Gaussian. Then the last two steps correspond to a per-pixel intersection test between a ray and the Gaussians, and rasterization process. The subset $\{\alpha_i\}$ corresponds to the Gaussians that are projected onto the image plane of camera c at time t . The subset $\{\beta_j\}$ corresponds to the Gaussians hit by the ray $R_{c,d}^t$ cast for a pixel.

The key learnable parameter is θ . It is ideal to make a full Bayesian inference on the posterior distribution of θ , since there is more than one set of θ s which can provide good reconstruction. In practice, this is extremely challenging due to the large number of θ . Models such as Hierarchical Dirichlet Processes could describe our generative process by assuming conjugate priors (e.g. Dirichlet-Multinomial), so that intermediate latent variables such as α , β can be marginalized. However, some steps of the generative process are dictated by light transport which cannot be easily described by probabilistic distributions. Furthermore, even if we forcefully used a full probabilistic

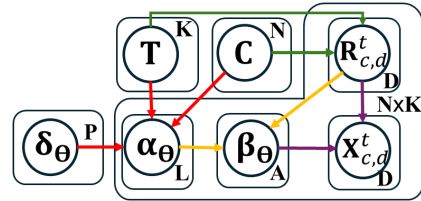


Fig. 2. A graphical model for GraphiXS. The colors correspond to the 4 steps of the generative process (1: red, 2: green, 3: yellow, 4: purple)

model, the optimization would involve intensive sampling or large-scale variational inference [Van de Maele et al. 2024], both being prohibitively slow in the presence of millions of θ s. Therefore, we choose Maximum a Posteriori (MAP):

$$\arg \max_{\theta} P(X | R, \beta, \alpha, C, T, \delta_{\theta}) P(\delta_{\theta}) \quad (4)$$

where we assume uninformative priors for C and T . Despite not directly modeling their priors, we do implicitly consider their influence on the distribution of the components as random variables, explained later. We first factorize the likelihood following the graphical model:

$$\begin{aligned} P(X | R, \beta, \alpha, C, T, \delta_{\theta}) &= P(X | \bullet) \\ &= P(X | \beta, R) P(\beta | \alpha, R) P(R | C, T) P(\alpha | \delta_{\theta}, C, T), \end{aligned} \quad (5)$$

where we use \bullet to represent variables in the condition for brevity. Also, among the possible options for instantiating δ in GraphiXS, e.g. Gaussians, Student's-t, Beta, etc., we assume the component is a distribution parameterized by basic attributes including mean μ , variance Σ , color s , opacity o , and other dynamics related attributes introduced later. Although this assumption excludes free-form parameterizations such as shapes [Held et al. 2025], it is still valid for many GS frameworks. Below, we give the key equations of our instantiations of different distributions in Eq. (5) and provide the details in the supplementary material (SM).

3.3 Probabilistic Image Reconstruction

$P(X | \bullet)$ represents the image generative process with 4 distributions. As mentioned, some of the steps are dictated by the light transport and are deterministic. So we realize them as deterministic processes following existing practice and introduce stochasticity in the others:

$$P(X | \bullet) = \underbrace{P(X | \beta, R)}_{\text{rasterization}} \underbrace{P(\beta | \alpha, R)}_{\text{per-pixel component}} \underbrace{P(R | C, T)}_{\text{per-pixel ray}} \underbrace{P(\alpha | \delta_{\theta}, C, T)}_{\text{per-image component}} \quad (6)$$

Following 3DGS [Kerbl et al. 2023], we realize $P(X | \beta, R)$ as rasterization:

$$Ras(X; \beta, R) = \sum_{i=1}^N \lambda_i \beta_{2D,i}(X), \quad \lambda_i = s_i o_i \prod_{j=1}^{i-1} (1 - o_j \beta_{2D,j}(X)) \quad (7)$$

where β_{2D} is a component projected onto the image space. Similarly, $P(\beta | \alpha, R) = \text{Intersect}(R, \alpha)$ is the per-pixel intersection test to identify the relevant components β . $P(R | C, T) = \text{RayCasting}(C, T)$ is ray casting which describes a ray R from a camera c into the space at time t . Combining the first three steps gives:

$$X = Ras(X; \text{Intersect}(R, \alpha), \text{RayCasting}(C, T)) = Ras(X; \bullet), \quad (8)$$

which is not a distribution and therefore cannot be directly used for MAP. So we use an energy-based distribution [Zhu et al. 2025]:

$$\begin{aligned} P(I | \beta, R, \alpha, C, T) &\propto \exp\left(-\sum_c^M \sum_t^K L_{img}(I_c^t)\right) \\ L_{img} &= (1 - \epsilon_{D-SSIM}) L_1 + \epsilon_{D-SSIM} L_{D-SSIM} \\ &\quad + \epsilon_o \sum_i ||o_i||_1 + \epsilon_{\Sigma} \sum_i \sum_j ||\sqrt{\lambda_{i,j}}||_1 \end{aligned} \quad (9)$$

where L_1 and L_{D-SSIM} are the L_1 norm and the structural similarity loss between the reconstructed image (by Eq. (8)) and the ground-truth. λ s are the eigenvalues of Σ . The regularization applied to the opacity ensures that the opacity is big only when a component is absolutely needed. The regularization on λ ensures the model uses components as spiky as possible (i.e. small variances). Together, the regularization terms minimize the needed number of components.

Next, since there are theoretically an infinite number of configurations of θ s which can reconstruct the same radiance field, we argue that it is important to impose preferences on well-behaved θ s. We impose this preference as stochasticity where well-behaved components have higher probabilities, via:

$$P(\alpha | \delta_{\theta}, C, T) = E\{P(r_{c,d}^t | \alpha)\} \approx \frac{\sum_c^M \sum_t^K \sum_d^D P(r_{c,d}^t | \alpha)}{\sum_p^N \sum_c^M \sum_t^K \sum_d^D P(r_{c,d}^t | \delta_{\theta_p})} \quad (10)$$

where $P(r_{c,d}^t | \alpha)$ and $P(r_{c,d}^t | \delta_{\theta_p})$ are the likelihoods of a ray $r_{c,d}^t$ from camera c at time t with respect to a component α and δ_{θ_p} . M, K, D, N are the total number of cameras, frames, pixels per image, and components. $P(r_{c,d}^t | \delta_{\theta_p})$ is the soft visibility of δ_{θ_p} to a pixel $x_{c,d}^t$. When δ_{θ_p} has low variance and high $P(r_{c,d}^t | \delta_{\theta_p})$, δ_{θ_p} is highly visible to $X_{c,d}^t$. Overall, in Eq. (10), the numerator is the soft visibility of component α to all pixels of all images across all times, while the denominator is the sum of all the soft visibility of all components. Therefore, we call $P(\alpha | \delta_{\theta}, C, T)$ the component confidence. A component with high confidence is more visible to all pixels in all frames relative to other components.

Aside from the visibility of components to cameras in time, conversely, $P(\alpha | \delta_{\theta}, C, T)$ also implicitly considers the influence of the distributions of C and T on the components. This is important for accommodating sparse views or missing frames. Maximizing this probabilistic distribution means placing components with high probabilities in the overlapped visible regions of multiple cameras and times. If the data is missing from any camera or time, the correctly placed components will be able to make good ‘guesses’ of the 4D radiance field for the missing cameras and frame times, hence robust to these uncertainties.

3.4 Prior for Component Parameters

After the likelihood function, we model the prior $P(\delta_{\theta})$ by modeling the distribution of the parameter θ . We assume our components move in space and time, and parameterize $P(\theta)$ to capture their dynamics, assuming $\theta(t)$ is function of t :

$$P(\theta(t)) = P(\theta(1)) \prod_{t=2}^K P(\theta(t) | \theta(t-1)) \quad (11)$$

The full specification of $\theta = \{\mu, \Sigma, o, sh, g, u, v, a, j, s\}$ includes a set of learnable parameters of the components, where μ, Σ are the mean and covariance. o is the base opacity. sh denotes its color represented through spherical harmonics. In time, a component can appear at any time g and last for a period of time u . In addition, we also introduce other dynamics related variables v, a, j, s where are detailed later.

We do not treat all variables in θ as functions of time explicitly. Instead, we explicitly model μ as it is the main variable governing the location of the components. We also make sh dependent on μ . The rest is learned independently. Note that the current θ specification is

the minimal set of variables to model component dynamics. They are broadly shared in multiple types of components, *e.g.* Gaussian, Beta, Student's-t. There might be other parameters for certain choices of components, such as the control parameter in Student's-t. In this case, these additional parameters are learned independently.

First, we model $\mu(t)$ as Brownian motions:

$$\frac{d\mu}{dt} = f(\mu, t) + \mathcal{N}(0, \epsilon^2 \mathbf{I}) \quad (12)$$

where \mathcal{N} is a Normal distribution with standard deviation ϵ . \mathbf{I} is identity matrix. The reason is that we observe that the motions of objects are arbitrary and there is even no guarantee of motion smoothness. Therefore, it is crucial to be able to learn arbitrary and even potentially discontinuous motions. Discretizing Eq. (12) in time gives:

$$\mu(t) = \mu(t-1) + f(\mu, t) \Delta t + \mathcal{N}(0, \epsilon^2 \mathbf{I}) \Delta t \quad (13)$$

where the dynamics is governed by $f(\mu, t)$. One simple way of modeling $f(\mu, t)$ is to consider the velocity of the components as in existing methods [Wu et al. 2024]. However, to also consider highly discontinuous motions, we learn several orders of motion derivatives, velocity v , acceleration a , jerk j and snap s :

$$f(\mu, t) \Delta t = v(t - \mu_t) + \frac{1}{2} a(t - \mu_t)^2 + \frac{1}{6} j(t - \mu_t)^3 + \frac{1}{24} s(t - \mu_t)^4 \quad (14)$$

Besides, we also design priors on other parameters. This is because MAP for GraphiXS involves millions of parameters. It can easily overfit without prior knowledge to regulate the variables. First, we impose a prior on the base opacity o following [Wang et al. 2025b]:

$$P(o) \propto \frac{1}{N} \sum_1^N o^2 \exp\left(-\frac{1}{2} \frac{t-g}{u}\right) \psi(\cdot), \quad (15)$$

where N is the total number of components, and $\psi(\cdot)$ denotes the evaluated response of the splatting distribution. The inputs to $\psi(\cdot)$ depend on the chosen component and its associated parameters. For Gaussian, $\psi(\cdot)$ is evaluated using the mean and variance, whereas for Student's-t we additionally include its control parameter v . Please see the SM for details. Overall this prior penalizes excessively large base opacity values.

Next, we also impose a prior on Σ :

$$P(\Sigma_p^t) \propto \exp(-\lambda_\sigma \frac{1}{N^t} \sum_p^t \|\Sigma_p^t - \hat{\Sigma}_p^t\|_F^2) \quad (16)$$

where Σ_p^t is the covariance of the p th component at time t , λ_σ is a weight, $\hat{\Sigma}_p^t$ is the mean covariance of all components at time t , $\|\cdot\|_F$ is the Frobenius norm, N^t is the total number of components at time t . This prior prefers small shape disparities between components.

We also place a prior on the dynamics related variables:

$$P(v_p^t, a_p^t, j_p^t, s_p^t) \propto \exp(-\lambda_h \frac{1}{P^t} \sum_p^t \sqrt{|\det(\Sigma_p^t)|} (||v_p^t||^2 + ||a_p^t||^2 + ||j_p^t||^2 + ||s_p^t||^2)) \quad (17)$$

which prefers slowly and smoothly moving components. More importantly, it is weighted by the volume proxy of the component $|\det(\Sigma_p^t)|$, so that the larger the component is, the slower and smoother its motion should be. This is based on the observation that larger

components cover a large area in space. These tend to be in the static background, so they should not move too often and too quickly.

Finally, combining Eq. (12-17), Eq. (11) becomes:

$$P(\theta(t)) = P(o)P(\mu(1)) \prod_{t=2}^K \mathcal{N}(\mu(t-1) + f(\mu, t), \epsilon^2 \mathbf{I}) \prod_{t=1}^K P(v^t, a^t, j^t, s^t) P(\Sigma^t) \quad (18)$$

with the rest parameters learned directly without stochasticity. $P(\theta(1))$ is realized by Eq. (9) for the first frame.

3.5 Objective Function and Optimization

Finally, with Eq. 9-18, we have all the elements for MAP (Eq. (4)):

$$\begin{aligned} & \arg \max_{\theta} \log P(X | R, \beta, \alpha, C, T, \theta) P(\theta) \\ & \Leftrightarrow \arg \min_{\theta} -\log [P(X | R, \beta, \alpha, C, T, \theta) P(\theta)] \end{aligned} \quad (19)$$

where the final loss function is:

$$\mathcal{L}_{\text{full}} = \underbrace{\mathcal{L}_{\text{img}}}_{-\log P(I|\bullet)} + \underbrace{\mathcal{L}_{\alpha}}_{-\log P(\alpha|\bullet)} + \underbrace{\mathcal{L}_{\theta}}_{-\log P(\theta)} \quad (20)$$

For optimization, we use Stochastic Gradient Hamiltonian Monte Carlo (SGHMC) [Zhu et al. 2025], which injects momentum and controlled stochasticity into gradient updates. In addition, we design component addition/removal sampling and initialization strategies for GraphiXS. Details can be found in the SM.

4 Experiments

Dataset. To evaluate GraphiXS, we need to mimic different types of data uncertainty, which requires the original dataset to have enough cameras, views with good coverage, sufficiently high frequency, *etc.* Based on the criteria, we choose the Neural 3D Video (N3DV) dataset [Li et al. 2022]. Following prior work [Lee et al. 2024; Wang et al. 2025b; Wu et al. 2024; Yang et al. 2024b], we down-sample all videos to 1352×1014 for both training and evaluation. We consistently hold out the first camera as the test view across all experimental settings. We evaluate reconstruction quality on this view over a duration of 300 consecutive frames at 30 FPS.

Metrics. We use PSNR (Peak Signal-to-Noise Ratio), DSSIM (Dis-similarity Structural Similarity Index Measure), and LPIPS (Learned Perceptual Image Patch Similarity) [Zhang et al. 2018]. For LPIPS, we report results computed using AlexNet. DSSIM is derived from the multi-scale structural similarity (MS-SSIM) index by converting similarity to a dissimilarity measure and scaled by a factor of 0.5.

Baseline Methods. We choose a representative set of state-of-the-art methods as baselines including 4DGS-1 [Yang et al. 2024b], 4DGS-2 [Wu et al. 2024], Ex4DGS [Lee et al. 2024], and FreeTimeGS [Wang et al. 2025b]. We use their official open-source implementations when available, otherwise our own implementation (for FreeTimeGS [Wang et al. 2025b]). For fair comparison, we train all models from scratch and run them 3 times and report the average. We color the best and second best results in green and yellow respectively. We only report results for the whole dataset in the main paper and include more detailed results and analysis in the SM.

Table 1. Comparison under standard setting.

Method	PSNR \uparrow	DSSIM \downarrow	LPIPS \downarrow
4DGS-1	31.18	0.015	0.051
4DGS-2	30.52	0.019	0.060
Ex4DGS	31.71	0.015	0.050
FTGS	31.55	0.016	0.047
Ours (GraphiGS)	31.78	0.015	0.044
Ours (GraphiTS)	32.02	0.015	0.043

Uncertainty Settings. We design several settings for multiple types of commonly seen data uncertainty. Standard Setting uses exactly the same setting as the baseline methods, regarded as without any data uncertainty. Sparse Views represents missing cameras. Sparse Frames represents only low frequency cameras are used. Unsynchronized Cameras represents a group of cameras which are not synchronized. Faulty Cameras represents a system with random camera malfunctions. Together these settings cover a wide range of possible scenarios where data uncertainty is induced into the data.

Instantiation and Generalization. GraphiXS does not assume specific components, so we instantiate it with two components to show its generality. The first is Student’s-t (GraphiTS) and the second is approximate Gaussian (GraphiGS) by fixing the control parameter of Student’s-t to a large value. In addition, we show that GraphiXS can be used to ‘upgrade’ existing 4DGS methods.

4.1 Comparison under Standard Setting

We show the numerical results in Tab. 1. Overall, the DSSIM for most methods are similar showing all methods capture the structure of images well in reconstruction. Both GraphiTS and GraphiGS outperform existing methods, mainly on PSNR and LPIPS. This is somewhat surprising, as the camera angles in N3DV are dense *e.g.* little data uncertainty, so one would assume further modeling of data uncertainty is redundant. However, the experiments demonstrate that even with the full observations, explicitly considering data uncertainty can further enhance the reconstruction quality. We show one visual result in Fig. 3. This is a difficult scene. One example is that one hand of the person holding a tong moves quickly from time to time, causing visual blur. This motion involves constantly stirring the spinach in random manner both spatially and in terms of its dynamics, causing motion blur. So capturing the high-order dynamics is crucial. Therefore, comparatively GraphiXS reconstructs clearer structures of the hand and tong with details, demonstrating the dynamics of the components are learned well.

4.2 Comparison under Sparse Views

In Sparse Views, we randomly remove 10%, 30%, and 50% of the training cameras, causing view gaps. Table 2 shows the numerical comparison. Overall, GraphiXS outperforms or is in par with other methods across all metrics. Due to the dense nature of the cameras in N3DV, a 10% reduction of the cameras does not challenge the methods, sometimes even improve the results (*e.g.* PSNR in 4DGS-1, 4DGS-2 and Ex4DGS). Further analysis suggests that the difference might be due to the randomness in the training for different methods, which might cause bigger variances in different runs in some methods but overall give similar results to the Standard Setting. When

Table 2. Comparison at different levels of spatial sparsity.

Method	10%			30%			50%		
	PSNR \uparrow	DSSIM \downarrow	LPIPS \downarrow	PSNR \uparrow	DSSIM \downarrow	LPIPS \downarrow	PSNR \uparrow	DSSIM \downarrow	LPIPS \downarrow
4DGS-1	31.37	0.015	0.049	29.11	0.024	0.058	28.54	0.027	0.068
4DGS-2	31.00	0.016	0.057	28.68	0.024	0.069	27.99	0.029	0.074
Ex4DGS	30.94	0.016	0.051	28.86	0.026	0.064	28.33	0.028	0.067
FTGS	31.38	0.016	0.047	29.04	0.026	0.063	28.06	0.031	0.072
Ours (GraphiGS)	31.73	0.016	0.044	29.35	0.025	0.058	28.60	0.026	0.066
Ours (GraphiTS)	31.62	0.016	0.046	29.41	0.024	0.061	28.56	0.027	0.067

Table 3. Comparison at different levels of temporal sparsity.

Method	20 FPS			10 FPS		
	PSNR \uparrow	DSSIM \downarrow	LPIPS \downarrow	PSNR \uparrow	DSSIM \downarrow	LPIPS \downarrow
4DGS-1	31.26	0.015	0.049	30.72	0.016	0.051
4DGS-2	30.46	0.016	0.058	31.01	0.016	0.059
Ex4DGS	31.39	0.015	0.050	31.15	0.016	0.053
FTGS	31.39	0.017	0.046	31.36	0.017	0.046
Ours (GraphiGS)	31.88	0.015	0.043	31.87	0.015	0.044
Ours (GraphiTS)	31.62	0.015	0.043	31.63	0.015	0.044

dropping 30% and 50% of the cameras, all metrics start to deteriorate, showing Sparse Views induces major data uncertainty. Across all three settings, GraphiXS achieves the best in 8 of 9 experiments and the second best in 1 experiment. We show one visual result in Fig. 1 Left and more results in Fig. 4. When more cameras are missing, it becomes more challenging for all methods where GraphiXS is affected the least.

4.3 Comparison under Sparse Frames

In Sparse Frames, we reduce the frame rate of the training cameras from 30 FPS to 20 and 10 FPS while still evaluating the scene at 30 FPS causing time sparsity. Table 3 shows the numerical results for both settings. Overall GraphiXS outperforms other methods. Different from Sparse Views, Sparse Frames mimics low frequency cameras which are not suitable for recording fast motions. Since motions in N3DV are generally not fast, and all methods have dedicated parts to learn the dynamics of the components, Sparse Frames is generally less challenging than Sparse Views.

Furthermore, the key difference between different methods stem from how dense in time they require samples to be. However individual model behaviors do not share the same pattern. For the baseline methods, when FPS is lower, the results become worse as expected. The only exception is 4DGS-2 which is slightly improved. Our speculation is that since 4DGS-2 exhaustively learns pair-wise relationships between the x , y , z coordinates of the Gaussian mean and time t , there is a chance their network overfits when the sample density in time is too high. So down-sampling actually improves the results. Last, GraphiGS does not deteriorate from Standard Setting, GraphiTS deteriorates at 20 FPS but not further in 10 FPS. We show one visual result in Fig. 1 Middle and more results in Fig. 5.

4.4 Comparison under Unsynchronized Cameras

In data capture, synchronizing cameras require extra hardware, software and calibration effort. So we test if methods could work with

Table 4. Comparison under different levels of Unsynchronization.

Method	10% @ 20 FPS			50% @ 20 FPS		
	PSNR↑	DSSIM↓	LPIPS↓	PSNR↑	DSSIM↓	LPIPS↓
4DGS-1	31.57	0.015	0.049	31.54	0.015	0.050
4DGS-2	30.68	0.016	0.059	30.92	0.016	0.059
Ex4DGS	31.34	0.016	0.050	31.01	0.016	0.051
FTGS	31.44	0.017	0.047	31.34	0.017	0.047
Ours (GraphiGS)	31.78	0.015	0.044	31.76	0.015	0.044
Ours (GraphiTS)	31.87	0.014	0.043	31.85	0.015	0.043

Table 5. Comparison with Random Faulty Cameras.

Method	Setting 1			Setting 2		
	PSNR↑	DSSIM↓	LPIPS↓	PSNR↑	DSSIM↓	LPIPS↓
4DGS-1	30.77	0.017	0.051	30.31	0.020	0.055
4DGS-2	30.56	0.018	0.061	29.78	0.021	0.065
Ex4DGS	30.52	0.019	0.053	30.03	0.020	0.056
FTGS	30.46	0.020	0.051	29.90	0.026	0.051
Ours (GraphiGS)	30.90	0.018	0.048	30.39	0.020	0.052
Ours (GraphiTS)	30.79	0.019	0.050	30.18	0.021	0.053

unsynchronized cameras. We simulate this scenario by setting cameras at different FPS. We randomly select 10% and 50% of cameras and reduce their FPS from 30 to 20, yielding 2 settings with two levels of partial temporal sparsity. Table 4 shows the results. Overall, we find Unsynchronized Cameras is an easier setting for all methods compared with Sparse Views and Sparse Frames. This is expected as all methods learn the dynamics of the components which does not require observations to be available for arbitrary time. Unsynchronized Cameras could be a bigger issue if cameras are not dense in space where every frame from every camera is crucial in capturing the motions. But in N3DV, all the cameras are in front of the person. Overall, GraphiXS gives the best results.

4.5 Comparison under Faulty Cameras

During data recording, any camera can malfunction which will cause a combination of all the types of the data uncertainty before this section. This data uncertainty spans across space and time. We design two settings to simulate Faulty Camera. Both settings aggregate the previous parameters, resulting in total space-time sparsities of approximately 13% for Setting 1 and 37% for Setting 2. Table 5 shows the numerical results for both settings. One visual example is shown in Fig. 1 Right and more are in Fig. 6.

4.6 GraphiXS as an Upgrade

GraphiXS is not only a specific method, but a framework that can be used to ‘upgrade’ other methods. This involves turning their deterministic models into probabilistic ones, using formulations similar to Eq. (9), then modeling stochasticity. The former step varies depending on the specific method, and the latter step is to add our stochastic components such as $P(\alpha | \theta, C, T)$ and $P(\Sigma_p^t)$. We directly show results here and give the details in the SM. We use the Standard Setting and the Faulty Camera setting as it includes all types of data uncertainty. Among the latest methods, we choose FTGS [Wang et al. 2025b] and Table 6 shows the numerical results. One visual example is shown in Fig. 7.

Table 6. Comparison in before and after upgrade for FTGS across Standard and Faulty Camera settings.

Method	Standard			Faulty Cam 1			Faulty Cam 2		
	PSNR↑	DSSIM↓	LPIPS↓	PSNR↑	DSSIM↓	LPIPS↓	PSNR↑	DSSIM↓	LPIPS↓
FTGS	31.55	0.016	0.047	30.46	0.020	0.051	29.90	0.026	0.051
FTGS UG	31.61	0.016	0.044	30.80	0.019	0.050	30.20	0.021	0.054

4.7 Ablation Study

Since we decompose GraphiXS into distributions (Eq. (5)) and propose various parameterization for each distribution, we show their respective effectiveness. The key distributions include the Higher Order Dynamics (Eq. (12)) and the component confidence $P(\alpha | \delta_\theta, C, T)$ (Eq. (10)). Therefore, we conduct an ablation study on GraphiGS under the two settings of Faulty Cameras. We show the quantitative results in Table 7 and qualitative results in Fig. 8.

In general, removing any component will deteriorate the results. This is more obvious in Setting 2 which has a higher level of uncertainty. ‘W/O Higher Order Dynamics’ only considers the position and velocity of the component, which is a strategy for many existing 4DGS methods [Lee et al. 2024; Li et al. 2024; Wang et al. 2025b]. But the results clearly shows that considering higher order dynamics will improve the results. Furthermore, ‘W/O $P(\alpha | \theta, C, T)$ ’ shows that the component confidence part also improves the results. This part is designed to regulate component locations and shapes to make them visible to cameras in time. In other words, every component should maximize its utility to the whole model.

Table 7. Quantitative results of our ablation study on GraphiGS.

Method	Faulty Cams					
	Setting 1			Setting 2		
	PSNR↑	DSSIM↓	LPIPS↓	PSNR↑	DSSIM↓	LPIPS↓
W/O Higher Order Dynamics	30.84	0.019	0.049	30.03	0.021	0.054
W/O $P(\alpha \theta, C, T)$	30.74	0.019	0.051	30.04	0.022	0.054
Ours (GraphiGS)	30.90	0.018	0.048	30.39	0.020	0.052

5 Conclusion and Discussion

We have proposed the first probabilistic 4DGS framework, GraphiXS, that holistically considers multiple types of data uncertainty. GraphiXS is general in that it can be instantiated with different components or used to upgrade existing deterministic methods. Through exhaustive evaluation and comparison, we have demonstrated the effectiveness of GraphiXS. A major limitation is GraphiXS assumes the components are probabilistic distributions parameterized by a set of common parameters. This makes it unsuitable for upgrading methods with other types of components such as geometric primitives. Also, GraphiXS does not do full Bayesian inference, *i.e.* no posterior distribution learned for θ , which would be ideal given the stochastic nature of 4DGS models.

Acknowledgments

This work was supported in part by the Rabin Ezra Scholarship Trust (Charity No. 1116049), awarded to Doğa Yılmaz.

References

Tim Bailey and Hugh Durrant-Whyte. 2006. Simultaneous localization and mapping: part II. *IEEE robotics & automation magazine* 13, 3 (2006), 108–117.

Minh-Quan Viet Bui, Jongmin Park, Juan Luis Gonzalez Bello, Jaeho Moon, Jihyong Oh, and Munchurl Kim. 2025. MoBGS: Motion Deblurring Dynamic 3D Gaussian Splatting for Blurry Monocular Video. *arXiv preprint arXiv:2504.15122* (2025).

Pinxuan Dai, Jiamin Xu, Wenxiang Xie, Xinguo Liu, Huamin Wang, and Weiwei Xu. 2024. High-quality surface reconstruction using gaussian surfels. In *ACM SIGGRAPH 2024 conference papers*. 1–11.

Junli Deng, Ping Shi, Qipei Li, and Jinyang Guo. 2025. DynaSplat: Dynamic-Static Gaussian Splatting with Hierarchical Motion Decomposition for Scene Reconstruction. *arXiv preprint arXiv:2506.09836* (2025).

Hugh Durrant-Whyte and Tim Bailey. 2006. Simultaneous localization and mapping: part I. *IEEE robotics & automation magazine* 13, 2 (2006), 99–110.

Guofeng Feng, Siyan Chen, Rong Fu, Zimu Liao, Yi Wang, Tao Liu, Boni Hu, Lining Xu, Zhihui Pei, Hengjie Li, et al. 2025. Flashgs: Efficient 3d gaussian splatting for large-scale and high-resolution rendering. In *Proceedings of the Computer Vision and Pattern Recognition Conference*. 26652–26662.

Qiankun Gao, Yanmin Wu, Chengxiang Wen, Jiarui Meng, Luyang Tang, Jie Chen, Ronggang Wang, and Jian Zhang. 2024. Relays: Reconstructing dynamic scenes with large-scale and complex motions via relay gaussians. *arXiv preprint arXiv:2412.02493* (2024).

Zhongpai Gao, Benjamin Planche, Meng Zheng, Anwesa Choudhuri, Terrence Chen, and Ziyuan Wu. 2025. 7DGs: Unified Spatial-Temporal-Angular Gaussian Splatting. *arXiv preprint arXiv:2503.07946* (2025).

Fengzhi Guo, Chih-Chuan Hsu, Sihao Ding, and Cheng Zhang. 2025. Uncertainty Matters in Dynamic Gaussian Splatting for Monocular 4D Reconstruction. *arXiv preprint arXiv:2510.12768* (2025).

Abdullah Hamdi, Luke Melas-Kyriazi, Jinjie Mai, Guocheng Qian, Ruoshi Liu, Carl Vondrick, Bernard Ghanem, and Andrea Vedaldi. 2024. Ges: Generalized exponential splatting for efficient radiance field rendering. In *Proceedings of the IEEE/CVF Conference on Computer Vision and Pattern Recognition*. 19812–19822.

Jan Held, Renaud Vandegheen, Abdullah Hamdi, Adrien Deliege, Anthony Cioppa, Silvio Giancola, Andrea Vedaldi, Bernard Ghanem, and Marc Van Droogenbroeck. 2025. 3D convex splatting: Radiance field rendering with 3D smooth convexes. In *Proceedings of the Computer Vision and Pattern Recognition Conference*. 21360–21369.

Binbin Huang, Zehao Yu, Anpei Chen, Andreas Geiger, and Shenghua Gao. 2024. 2d gaussian splatting for geometrically accurate radiance fields. In *ACM SIGGRAPH 2024 conference papers*. 1–11.

Yoonwoo Jeong, Junmyeong Lee, Hoseung Choi, and Minsu Cho. 2024. RoDyGS: Robust Dynamic Gaussian Splatting for Casual Videos. *arXiv preprint arXiv:2412.03077* (2024).

Yanqin Jiang, Li Zhang, Jin Gao, Weimin Hu, and Yao Yao. 2023. Consistent4d: Consistent 360 $\{\deg\}$ dynamic object generation from monocular video. *arXiv preprint arXiv:2311.02848* (2023).

Bernhard Kerbl, Georgios Kopanas, Thomas Leimkühler, and George Drettakis. 2023. 3D Gaussian splatting for real-time radiance field rendering. *ACM Trans. Graph.* 42, 4 (2023), 139–1.

Bernhard Kerbl, Andreas Meuleman, Georgios Kopanas, Michael Wimmer, Alexandre Lanvin, and George Drettakis. 2024. A hierarchical 3d gaussian representation for real-time rendering of very large datasets. *ACM Transactions on Graphics (TOG)* 43, 4 (2024), 1–15.

Shakiba Kheradmand, Daniel Rebain, Gopal Sharma, Weiwei Sun, Yang-Che Tseng, Hossam Isack, Abhishek Kar, Andrea Tagliasacchi, and Kwang Moo Yi. 2024. 3d gaussian splatting as markov chain monte carlo. *Advances in Neural Information Processing Systems* 37 (2024), 80965–80986.

Hyunjin Kim, Haebeom Jung, and Jaesik Park. 2025. Metropolis-Hastings Sampling for 3D Gaussian Reconstruction. *arXiv preprint arXiv:2506.12945* (2025).

Junoh Lee, ChangYeon Won, Hyunjun Jung, Inhwan Bae, and Hae-Gon Jeon. 2024. Fully explicit dynamic gaussian splatting. *Advances in Neural Information Processing Systems* 37 (2024), 5384–5409.

Tianye Li, Mira Slavcheva, Michael Zollhoefer, Simon Green, Christoph Lassner, Changil Kim, Tanner Schmidt, Steven Lovegrove, Michael Goesele, Richard Newcombe, et al. 2022. Neural 3d video synthesis from multi-view video. In *Proceedings of the IEEE/CVF conference on computer vision and pattern recognition*. 5521–5531.

Zhan Li, Zhang Chen, Zhong Li, and Yi Xu. 2024. Spacetime gaussian feature splatting for real-time dynamic view synthesis. In *Proceedings of the IEEE/CVF Conference on Computer Vision and Pattern Recognition*. 8508–8520.

Chin-Yang Lin, Cheng Sun, Fu-En Yang, Min-Hung Chen, Yen-Yu Lin, and Yu-Lun Liu. 2025. Longsplat: Robust unposed 3d gaussian splatting for casual long videos. In *Proceedings of the IEEE/CVF International Conference on Computer Vision*. 27412–27422.

Changkun Liu, Shuai Chen, Yash Bhalgat, Siyan Hu, Ming Cheng, Zirui Wang, Victor Adrian Prisacariu, and Tristan Braud. 2024. GS-CPR: Efficient camera pose refinement via 3d gaussian splatting. *arXiv preprint arXiv:2408.11085* (2024).

Rong Liu, Zhongpai Gao, Benjamin Planche, Meida Chen, Van Nguyen Nguyen, Meng Zheng, Anwesa Choudhuri, Terrence Chen, Yue Wang, Andrew Feng, et al. 2025a. Universal Beta Splatting. *arXiv preprint arXiv:2510.03312* (2025).

Rong Liu, Dylan Sun, Meida Chen, Yue Wang, and Andrew Feng. 2025b. Deformable beta splatting. In *Proceedings of the Special Interest Group on Computer Graphics and Interactive Techniques Conference Papers*. 1–11.

Saswat Subhajyoti Mallick, Rahul Goel, Bernhard Kerbl, Markus Steinberger, Francisco Vicente Carrasco, and Fernando De La Torre. 2024. Taming 3dgs: High-quality radiance fields with limited resources. In *SIGGRAPH Asia 2024 Conference Papers*. 1–11.

Hidenobu Matsuki, Riku Murai, Paul HJ Kelly, and Andrew J Davison. 2024. Gaussian splatting slam. In *Proceedings of the IEEE/CVF Conference on Computer Vision and Pattern Recognition*. 18039–18048.

Ben Mildenhall, Pratul P Srinivasan, Matthew Tancik, Jonathan T Barron, Ravi Ramamoorthi, and Ren Ng. 2021. Nerf: Representing scenes as neural radiance fields for view synthesis. *Commun. ACM* 65, 1 (2021), 99–106.

Richard A Newcombe, Shahram Izadi, Otmar Hilliges, David Molnyneaux, David Kim, Andrew J Davison, Pushmeet Kohli, Jamie Shotton, Steve Hodges, and Andrew Fitzgibbon. 2011. Kinectfusion: Real-time dense surface mapping and tracking. In *2011 10th IEEE international symposium on mixed and augmented reality*. Ieee, 127–136.

Jongmin Park, Minh-Quan Viet Bui, Juan Luis Gonzalez Bello, Jaeho Moon, Jihyong Oh, and Munchurl Kim. 2025. Splinegs: Robust motion-adaptive spline for real-time dynamic 3d gaussians from monocular video. In *Proceedings of the Computer Vision and Pattern Recognition Conference*. 26866–26875.

Albert Pumarola, Enric Corona, Gerard Pons-Moll, and Francesc Moreno-Noguer. 2021. D-nerf: Neural radiance fields for dynamic scenes. In *Proceedings of the IEEE/CVF conference on computer vision and pattern recognition*. 10318–10327.

Luca Savant, Diego Valsesia, and Enrico Magli. 2024. Modeling uncertainty for gaussian splatting. *arXiv preprint arXiv:2403.18476* (2024).

Johannes L. Schönberger et al. 2016. COLMAP: Structure-from-Motion and Multi-View Stereo. <https://colmap.github.io/>. Accessed: 2026-01-11.

Steven M Seitz, Brian Curless, James Diebel, Daniel Scharstein, and Richard Szeliski. 2006. A comparison and evaluation of multi-view stereo reconstruction algorithms. In *2006 IEEE computer society conference on computer vision and pattern recognition (CVPR'06)*, Vol. 1. IEEE, 519–528.

Shimon Ullman. 1979. The interpretation of structure from motion. *Proceedings of the Royal Society of London. Series B. Biological Sciences* 203, 1153 (1979), 405–426.

Toon Van de Maele, Ozan Çatal, Alexander Tschantz, Christopher L Buckley, and Tim Verbelen. 2024. Variational Bayes Gaussian Splatting. *arXiv preprint arXiv:2410.03592* (2024).

Rui Wang, Quentin Lohmeyer, Mirko Meboldt, and Siyu Tang. 2025a. Degauss: Dynamic-static decomposition with gaussian splatting for distractor-free 3d reconstruction. In *Proceedings of the IEEE/CVF International Conference on Computer Vision*. 6294–6303.

Yifan Wang, Peishan Yang, Zhen Xu, Jiaming Sun, Zhanhua Zhang, Yong Chen, Hujun Bao, Sida Peng, and Xiaowei Zhou. 2025b. FreeTimeGS: Free Gaussian Primitives at Anytime Anywhere for Dynamic Scene Reconstruction. In *CVPR*. <https://zju3dv.github.io/freetimegs>.

Guanjun Wu, Taoran Yi, Jiemin Fang, Lingxi Xie, Xiaopeng Zhang, Wei Wei, Wenyu Liu, Qi Tian, and Xinggang Wang. 2024. 4d gaussian splatting for real-time dynamic scene rendering. In *Proceedings of the IEEE/CVF conference on computer vision and pattern recognition*. 20310–20320.

Jianfeng Xiang, Zelong Lv, Sicheng Xu, Yu Deng, Ruicheng Wang, Bowen Zhang, Dong Chen, Xin Tong, and Jiaolong Yang. 2025. Structured 3d latents for scalable and versatile 3d generation. In *Proceedings of the Computer Vision and Pattern Recognition Conference*. 21469–21480.

Haozhe Xie, Zhaoxi Chen, Fangzhou Hong, and Ziwei Liu. 2025. Compositional generative model of unbounded 4D cities. *arXiv preprint arXiv:2501.08983* (2025).

Tianyi Xie, Zeshun Tong, Yuxing Qiu, Xuan Li, Yutao Feng, Yili Yang, and Chenfanfu Jiang. 2024. Physgaussian: Physics-integrated 3d gaussians for generative dynamics. In *Proceedings of the IEEE/CVF Conference on Computer Vision and Pattern Recognition*. 4389–4398.

Yueming Xu, Haochen Jiang, Zhongyang Xiao, Jianfeng Feng, and Li Zhang. 2024. Dg-slam: Robust dynamic gaussian splatting slam with hybrid pose optimization. *Advances in Neural Information Processing Systems* 37 (2024), 51577–51596.

Qitong Yang, Mingtao Feng, Zijie Wu, Weisheng Dong, Fangfang Wu, Yaonan Wang, and Ajmal Mian. 2025. Hierarchical Gaussian Mixture Model Splatting for Efficient and Part Controllable 3D Generation. In *Proceedings of the Computer Vision and Pattern Recognition Conference*. 11104–11114.

Ziyi Yang, Xinyu Gao, Wen Zhou, Shaohui Jiao, Yuqing Zhang, and Xiaogang Jin. 2024a. Deformable 3d gaussians for high-fidelity monocular dynamic scene reconstruction. In *Proceedings of the IEEE/CVF conference on computer vision and pattern recognition*. 20331–20341.

Zeyu Yang, Hongye Yang, Zijie Pan, and Li Zhang. 2024b. Real-time Photorealistic Dynamic Scene Representation and Rendering with 4D Gaussian Splatting. In

International Conference on Learning Representations (ICLR).

Doğa Yılmaz and Furkan Kıracı. 2023. Illumination-guided inverse rendering benchmark: Learning real objects with few cameras. *Computers & Graphics* 115 (2023), 107–121. doi:10.1016/j.cag.2023.07.002

Richard Zhang, Phillip Isola, Alexei A Efros, Eli Shechtman, and Oliver Wang. 2018. The unreasonable effectiveness of deep features as a perceptual metric. In *Proceedings of the IEEE conference on computer vision and pattern recognition*. 586–595.

Xiaoyu Zhou, Zhiwei Lin, Xiaojun Shan, Yongtao Wang, Deqing Sun, and Ming-Hsuan Yang. 2024. Drivinggaussian: Composite gaussian splatting for surrounding dynamic autonomous driving scenes. In *Proceedings of the IEEE/CVF conference on computer vision and pattern recognition*. 21634–21643.

Jialin Zhu, Jiangbei Yue, Feixiang He, and He Wang. 2025. 3D Student Splatting and Scooping. In *Proceedings of the Computer Vision and Pattern Recognition Conference*. 21045–21054.

Ruijie Zhu, Yanzhe Liang, Hanzhi Chang, Jiacheng Deng, Jiahao Lu, Wenfei Yang, Tianzhu Zhang, and Yongdong Zhang. 2024. Motions: Exploring explicit motion guidance for deformable 3d gaussian splatting. *Advances in Neural Information Processing Systems* 37 (2024), 101790–101817.

Matthias Zwicker, Hanspeter Pfister, Jeroen Van Baar, and Markus Gross. 2002. EWA splatting. *IEEE Transactions on Visualization and Computer Graphics* 8, 3 (2002), 223–238.

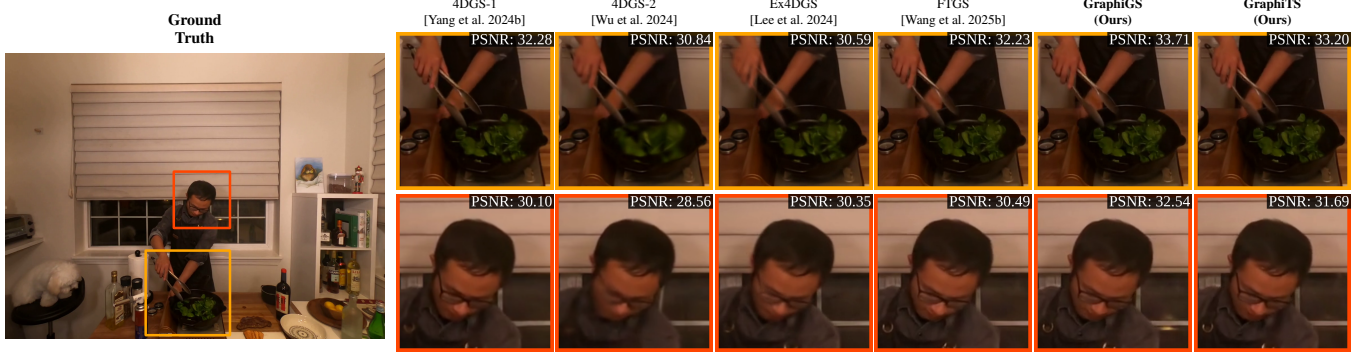


Fig. 3. Comparison under standard setting. Per-region PSNR scores are given at the top right of each image. Enlarged regions contain complex and fast motions e.g. the tongs motion. GraphiXS reconstruction is more clear and richer in details than other methods.

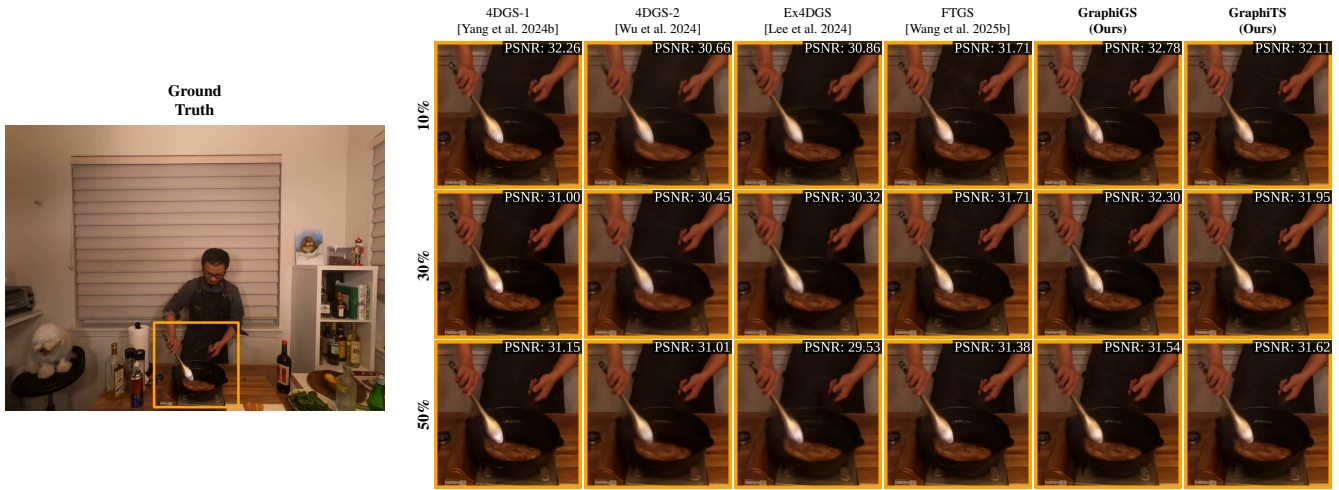


Fig. 4. Comparison under 10%, 30%, and 50% spatial sparsity. Per-region PSNR scores are given at the top right of each crop. GraphiXS is affected the least when the percentage of missing cameras increases.

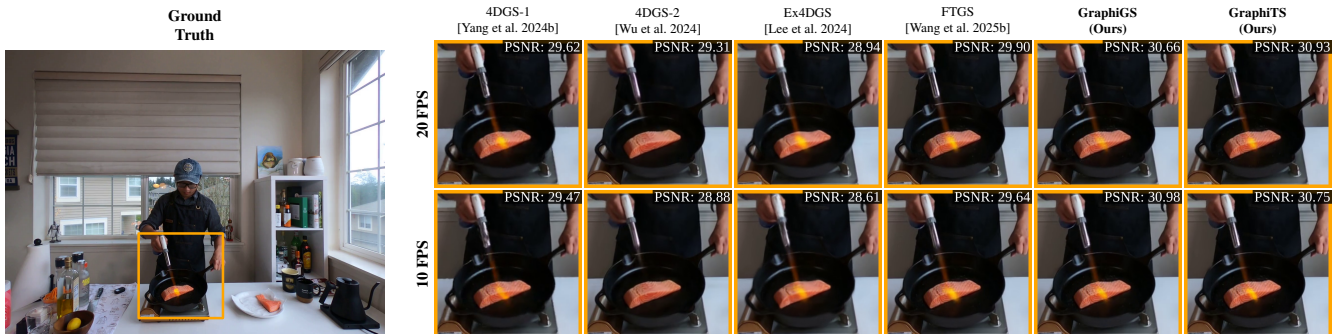


Fig. 5. Comparison under 20 FPS and 10 FPS temporal sparsity. Per-region PSNR scores are given at the top right of each crop. GraphiXS is affected the least when the training camera FPS drops.



Fig. 6. Comparison under faulty camera 1 and faulty camera 2 settings. Per-region PSNR scores are given at the top right of each crop. GraphiXS is affected the least when spatio-temporal sparsity is increased.



Fig. 7. Comparison of FTGS [Wang et al. 2025b] with and without upgrading under faulty camera 1 and 2 settings. Per-region PSNR scores are given at the top right of each crop. Upgrading FTGS using GraphiXS improves visual quality under various levels of spatio-temporal uncertainty.

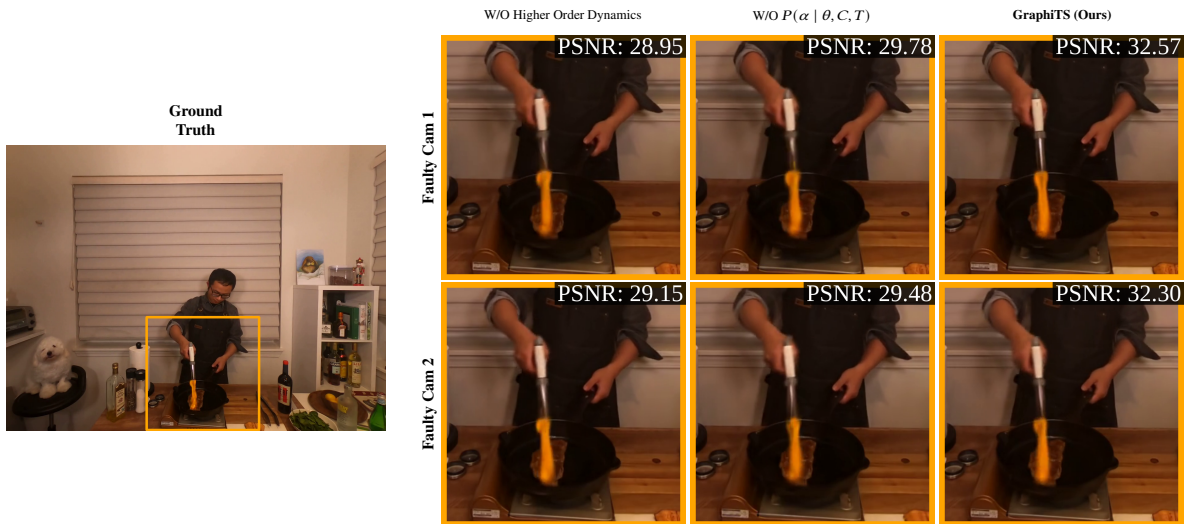


Fig. 8. Visual results of our ablation study. Per-region PSNR scores are given at the top right of each crop.